AGU100 ADVANCING EARTH AND SPACE SCIENCE

Geophysical Research Letters

RESEARCH LETTER
10.1029/2018GL079273

Key Points:
- The eastern and central Pacific types of El Niño produce different impacts on the NECC due to the distinct wind stress patterns associated with each
- The NECC intensifies and shifts southward in the central eastern Pacific during EP El Niño events but in the western central Pacific during CP El Niño events
- Ekman pumping and oceanic wave propagations link the different wind stress patterns to the distinct NECC changes

Supporting Information:
- Supporting Information S1

Correspondence to:
H. Zhou,
zhouhui@qdio.ac.cn

Citation:
Tan, S., & Zhou, H. (2018). The observed impacts of the two types of El Niño on the North Equatorial Countercurrent in the Pacific Ocean. *Geophysical Research Letters*, *45*, 10,493–10,500. https://doi.org/10.1029/2018GL079273

Received 19 JUN 2018
Accepted 14 SEP 2018
Accepted article online 19 SEP 2018
Published online 2 OCT 2018

The Observed Impacts of the Two Types of El Niño on the North Equatorial Countercurrent in the Pacific Ocean

Shuwen Tan[1,2] **and Hui Zhou**[1,2,3]

[1]CAS Key Laboratory of Ocean Circulation and Waves, Institute of Oceanology, Chinese Academy of Sciences, and Pilot National Laboratory for Marine Science and Technology, Qingdao, China, [2]University of Chinese Academy of Sciences, Beijing, China, [3]Center for Ocean Mega-Science, Chinese Academy of Sciences Qingdao Collaborative Innovation Center of Marine Science and Technology, Qingdao, China

Abstract This study investigates the interannual variations in the North Equatorial Counter Current (NECC) associated with the eastern Pacific and the central Pacific types of El Niño. Using observational analysis and ocean simulations, we show that the wind stress anomalies during the two El Niño types are of comparable amplitude but have different spatial structures, which results in significant and distinct variations in the NECC. The NECC shifts southward and intensifies during the developing phase of El Niño, but the variations are confined in the central eastern Pacific for the eastern Pacific type and the western central Pacific for the central Pacific type. These differences can be attributed to modulations in equatorial Kelvin wave and tropical Rossby wave propagation as well as Ekman pumping.

Plain Language Summary The North Equatorial Counter Current (NECC) is an eastward flowing surface current that transports a significant amount of water from the warm pool in the western Pacific to the east. Variations in the NECC exert profound effects on the tropical Pacific climate and need to be better understood. This study conducts statistical analyses and ocean model experiments to show that different flavors of El Niño can displace the NECC location and alter its intensity in distinct ways. The cause and the physical mechanisms behind the distinct impacts are identified and verified using specific El Niño events of each flavor. The findings reported in this study contribute to advance our understanding of El Niño diversity and its impacts on the circulation and variability of the Pacific Ocean.

1. Introduction

The North Equatorial Counter Current (NECC) is an eastward flowing surface current centered at 5–6°N in the Pacific Ocean (Donguy & Meyers, 1996; Reverdin et al., 1994; Wyrtki & Kendall, 1967; Yu et al., 2000). The NECC transports a significant amount (about 10–30 Sv) of surface water from the warm pool in the western Pacific to the east (Donguy & Meyers, 1996; Gouriou & Toole, 1993; Johnson et al., 2002; Philander et al., 1987; Wyrtki & Kendall, 1967) and plays an important role in shaping the tropical Pacific climate, in particular the equatorial asymmetry of the Intertropical Convergence Zone (Masunaga & L'Ecuyer, 2011; Richards et al., 2009).

The interannual variations in the NECC have been suggested to be closely connected to El Niño/Southern Oscillation (ENSO) events with larger transport and a southward shift of its axis during El Niño events (Delcroix et al., 1992; Hsin & Qiu, 2012; Johnson et al., 2002; Kessler & Taft, 1987; Meyers & Donguy, 1984; Wyrtki, 1979; Zhao et al., 2013). The underlying dynamics of the impact are associated with sea level anomalies (SLAs) generated by local wind anomalies and the accompanying westward propagating baroclinic Rossby waves in the western central tropical North Pacific Ocean (Delcroix et al., 1992; Hsin & Qiu, 2012; Kessler & Taft, 1987; Meyers & Donguy, 1984; Qiu & Joyce, 1992; Wyrtki, 1979; Yu et al., 2000; Zhao et al., 2013).

Recent studies have suggested that the El Niño can be separated into two different types based on the spatial distribution of sea surface temperature anomaly (SSTA; Ashok et al., 2007; Kao & Yu, 2009; Kug et al., 2009; Larkin & Harrison, 2005). These two types are often referred to as the eastern Pacific (EP) El Niño and central Pacific (CP) El Niño (Kao & Yu, 2009; Yu & Kao, 2007). The SSTAs during EP El Niños are centered more over the cold tongue, while the anomalies are centered closer to the dateline during CP El Niños. These different spatial patterns have suggested that these two types of El Niño may produce distinct impacts on the NECC. Hsin and Qiu (2012, hereinafter HQ12) examined this possibility by contrasting the NECC properties

composited separately for the two types of El Niño observed during 1959–2009. They concluded that the EP El Niño exerts a significant impact on the NECC, whereas the CP El Niño has little influence.

HQ12's conclusion can be dependent on the identification method used to select the EP and CP El Niño events for their composites. They use the identification method of Kug et al. (2009), which compares the relative magnitudes of the Niño3 and Niño4 SST indices to determine the El Niño type. Ren and Jin (2011) argued that the Niño3 and Niño4 indices are highly correlated with each other and may not be suitable for identifying the two types of El Niño. In order to overcome this problem, Kao and Yu (2009, hereafter KY09) proposed another method, which separates the two types of El Niño using a regression-empirical orthogonal function method and contrasts their surface/subsurface information. We have applied this method to classify the El Niño events used in HQ12 and obtained a different classification of their types (see supporting information Text S1 and Table S1). Five of the EP events identified in HQ12 are reclassified as CP events. This reclassification can affect the conclusions obtained by HQ12. This possibility is examined in this study first by repeating the composite analysis of HQ12 but using the method of KY09. Correlation and regression analysis, case studies, and forced model experiments are also used to further examine the impacts on the NECC. In contrast to HQ12, we find that the CP El Niño can also significantly impact the NECC but in ways that differ from the EP El Niño. The underlying dynamics for the distinct impacts are then explained using Rossby and Kelvin wave dynamics.

2. Data and Methodology

Observational and reanalysis data are used in this study for statistical analyses and to force an ocean model. The monthly averages of daily gridded merged absolute dynamic topography heights (MADT-H) and absolute geostrophic velocities (MADT-UV) are used to calculate the central location and intensity of the NECC. These two data products are provided by Aviso+ (http://www.aviso.altimetry.fr) and the Copernicus Marine Environment Monitoring Service (http://marine.copernicus.eu/). The data are available from January 1993 to December 2016 at a spatial resolution of 0.25° × 0.25°. The monthly data from January 1958 to December 2017 of the European Centre for Medium-Range Weather Forecasts ocean analysis/reanalysis system (ORA-S4; Balmaseda et al., 2013; Mogensen et al., 2012) are used. These data have a spatial resolution of 1° × 1° and 42 vertical levels and were archived from http://icdc.cen.uni-hamburg.de/1/projekte/easy-init/easy-init-ocean.html?no_cache=1. The monthly European Centre for Medium-Range Weather Forecasts Interim Reanalysis (ERA-Interim) wind data at 10 m from 1979 to 2016 are used to force a 1.5-layer reduced-gravity model. The wind data have a spatial resolution of approximately 80 km and are obtained from http://apps.ecmwf.int/datasets/ (Berrisford et al., 2011).

The Ocean Niño Index is defined as the 3-month running means of the Extended Reconstructed Sea Surface Temperature version 4 SSTA in the Niño 3.4 region (ftp://ftp.ncdc.noaa.gov/pub/data/cmb/ersst/v4/). The warm and cold phases of ENSO are defined as a minimum in the Ocean Niño Index lasting five consecutive months and surpassing a threshold of ±0.5 °C. Updated monthly EP and CP indices (EPI and CPI) are calculated by applying the regression-empirical orthogonal function method (Kao & Yu, 2009; Yu & Kim, 2010) to Extended Reconstructed Sea Surface Temperature version 3 data set (https://www.ess.uci.edu/~yu/2OSC/).

Anomalies in this study are defined as the deviations from the monthly climatology after being detrended. Since we focus on interannual variations in the NECC, a 13-month Lanczos low-pass filter is applied to the monthly anomalies for all data sets unless specified otherwise. A 10-year Lanczos low-pass filter is also applied on long-term data (i.e., ORA-S4 and ERA) to remove decadal signals. We follow HQ12 in calculating the intensity (INT) and central latitude (Y_{CM}) of the NECC during the period 1993–2016 using both the ORA-S4 data and MADT-UV data (see supporting information Text S2 for details of the calculation). A Student's *t* test (Livezey & Chen, 1983; Shi et al., 1997) is used to assess the statistical significance of the correlations for each data set, accounting for the reduced number of degrees of freedom imposed by the filters.

3. Results

Using the identification method of KY09, we find that two CP El Niños (1963/1964 and 1965/1966) and three mixed-type El Niños (1969/1970, 1986/1988, and 1991/1992) were classified as EP El Niños in HQ12 and used in their EP El Niño composite. To examine the sensitivity of their results to this difference in classification, we

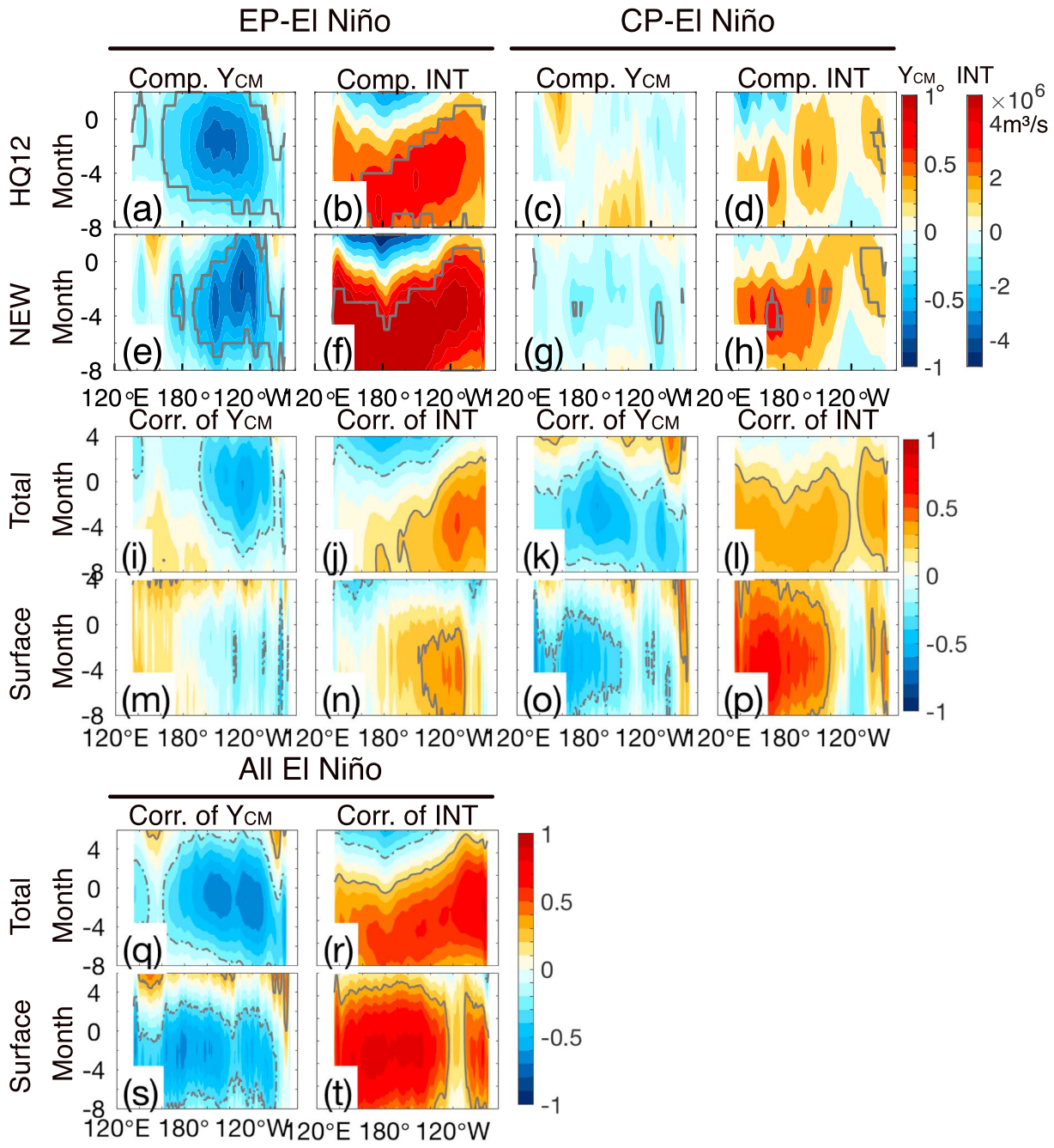

Figure 1. Variations in the NECC axis (Y_{CM}) and intensity (INT) associated with the EP and CP types of El Niño obtained from a composite analysis based on the HQ12 classification (a–d) and the classification used in this study (e–h). Lag correlations between anomalies in the total NECC Y_{CM} (INT) calculated from ORA-S4 and EP (CP) index (i–l) and between surface NECC Y_{CM} (INT) calculated from ADT-H data of Aviso+ and EP (CP) index (m–p), respectively. (q–t) The same as (i)–(l) but for Niño3.4 index. Negative month indicates Y_{CM}(INT) leading. Gray contours mark the 95% confidence levels (0.3 for Aviso data and 0.2 for ORA-S4 data) based on a two-tailed Student's *t* test. NECC = North Equatorial Counter Current; CP = central Pacific; EP = eastern Pacific.

repeated the composite analysis of HQ12 using the ORA-S4 data but with our type classification. Here the Y_{CM} and INT are calculated by integrating the positive zonal velocity from the surface down to the density level of 26-σ_θ to represent the whole depth of the NECC (Johnson et al., 2002). Our study focuses only on the developing to mature phase of El Niño events. The composites based on the classification of HQ12 are reproduced in Figures 1a–1d, which are consistent with Figures 3–6 of HQ12, both of which indicate that the EP El Niño has a strong impact on the NECC location and intensity while the CP El Niño has a weak impact.

The composites based on our classification (Figures 1e–1h) are similar to those based on HQ12's classification for the EP El Niño but different for the CP El Niño. Our composites show that the CP El Niño also has a strong impact on the NECC, but it is different from the EP El Niño. For the EP El Niño, the NECC axis begins to shift southward in the EP about 8 months before its mature phase (Figure 1e), which then extends westward as the event develops but is confined mostly to the east of 180°W. Meanwhile, the NECC intensifies first in the CP (around 180°E) and then spreads to the EP (Figure 1f). For the CP El Niño, the NECC axis also tends to shift southward and intensifies before the event peaks, but these variations are confined mostly to the western-central Pacific with relatively small amplitude (Figures 1g and 1h). These results differ from the insignificant variations in the NECC during CP events found by HQ12 (Figures 1c and 1d).

To further confirm the different impacts, we performed a lagged correlation analysis between the NECC properties (i.e., Y_{CM} and INT) and the EPI/CPI. The lagged correlation results (Figures 1i–1l) reproduce very well the composite results, except that the correlation results show more clearly that the strongest impacts occur over the tropical central eastern Pacific for the EP El Niño but over the western central Pacific for the CP El Niño. In particular, the NECC intensification is much more confined to the EP for the EP El Niño and to the western Pacific for the CP El Niño in the correlation results than in the composite results. Minor discrepancies exist between the composite and correlation results (cf. Figures 1f and 1j), correlation analyses by including or masking out La Niña events show consistent results, suggesting that these discrepancies may be caused by the different sample sizes involved in these two analysis methods (figure not shown).

Since in data-sparse regions of the ocean the ORA-S4 reanalysis is reduced to an ocean model simulation, the composite and correlation analyses using the reanalysis products can sometimes be biased. In order to address this concern, we also calculated Y_{CM} and INT using the altimeter data and then repeated the same lag correlation analysis of Figures 1i–1l. The results (Figures 1m–1p) are similar to those obtained using the ORA-S4 data, except that the region of correlation above the 95% confidence level in Figure 1m is smaller than that in Figure 1i, which may relate to the shorter time series of the altimeter measurements. The comparison provides observational evidence for the distinct impacts on the NECC by both types of El Niño. The correlations between INT and CPI for the whole depth NECC and surface NECC show quite different structures in the EP between 140°W and 100°W (cf. Figures 1p and 1l), which is mainly caused by variations in the surface NECC, and it is weakest and sometimes absent there (Johnson et al., 2002).

The lagged correlation between the NECC and the Niño3.4 index (Figures 1q–1t) reflects the combined impacts of the two types of El Niño on the NECC, which is characterized by a double-core structure in the correlations. This result indicates that it is important to stratify by El Niño type when discussing its impacts on the NECC.

To understand how the different El Niño impacts on NECC are produced, we regressed the anomalies of wind stress curl (WSCAs), dynamic height (ADT-HAs) and sea surface geostrophic zonal velocity (ADT-UAs) onto the EPI and CPI (Figure 2). During the development of the EP El Niño, pronounced westerly anomalies near the equator force downwelling Kelvin waves propagating toward the eastern equatorial Pacific. These waves can lift the sea surface height there (Figure 2c1), which later reach toward the South America Coast (Figure 2c2) and spread northward along the coast as the El Niño reaches its peak phase (Figures 2c3–2c5). The positive ADT-HAs at the equator increase the meridional pressure gradient, which strengthens and displaces southward the NECC through geostrophic balance in the EP (Figures 2e1–2e5). This effect of the EP El Niño on the NECC is confined to the central eastern Pacific due to the existence of a negative ADT-HA core to the west of the dateline (Figures 2c2–2c5) during the developing phase, which is caused by the positive Ekman pumping induced by the band-like positive WSCAs south of 5°N (Figures 2a2–2a5) and equatorial easterly anomalies west of 180°E near the equator (Figure 3a).

During the developing phase of the CP El Niño, the regression pattern for the WSCAs is very different from that during the EP El Niño. The pattern is dominated by a center of positive anomalies over the western Pacific north of the NECC and a center of negative anomalies to the east of the dateline near the equator (Figures 2b1–2b5). Correspondingly, the ADT-HAs are dominated by positive values south of the NECC and negative values in the western central Pacific north of the NECC (Figures 2d1–2d5). As the CP El Niño develops, the positive and negative values west of the dateline increase the meridional pressure gradient across the NECC, and hence, the NECC intensifies and shifts southward in the western central Pacific (Figures 2f1–2f5). The western edge of the positive ADT-HAs in the CP shows little sign of eastward

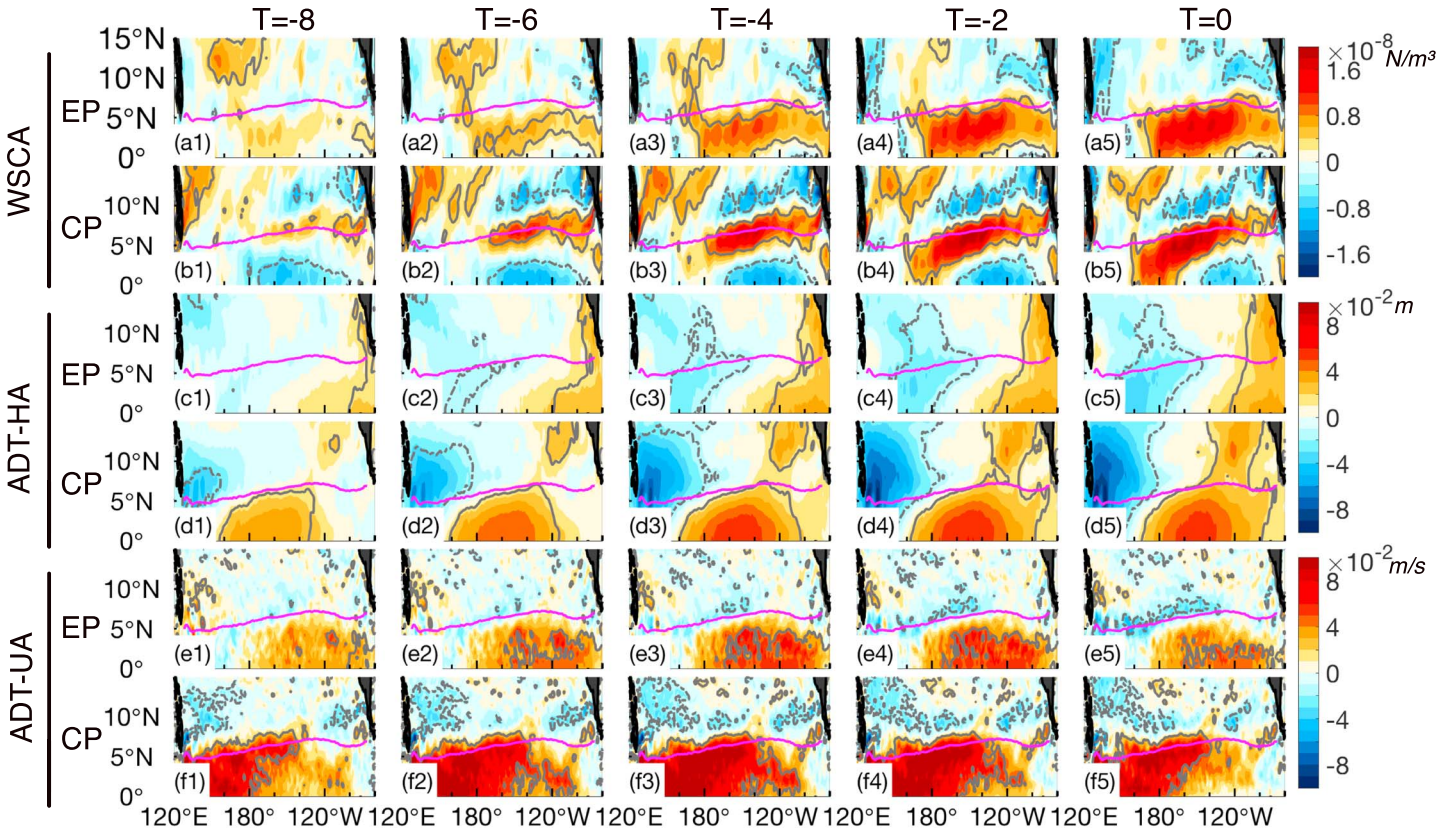

Figure 2. Evolution of the wind stress curl (a and b), ADT-H (c and d), and ADT-U (e and f) anomalies regressed onto the EP index (a, c, and e) and CP index (b, d, and f), respectively. Units are Newton per cubic meter in panels (a) and (b), meters in panels (c) and (d), and meters per second in panels (e) and (f), respectively. *T* denotes the lag month in the lagged regression, and negative lags indicate the regressed variables (i.e., WSCA, ADT-HA, and ADT-UA) lagging. The magenta lines denote the observed mean location (Y_{CM}) of the NECC during 1993–2016. The gray dashed lines indicate the values where the regression coefficients pass the 95% significance level based on a two-tailed Student's *t* test with Monte Carlo techniques. (0.3 for Aviso data and 0.23 for ERA data). CP = central Pacific; EP = eastern Pacific.

shrinking during the evolution of the CP El Niño. This stagnant feature of the ADT-HAs is consistent with the fact that there is no obvious propagation of SSTAs observed during the CP El Niño (KY09), which can be explained by the oceanic responses to the unique wind stress forcing during these events. The upwelling and downwelling Rossby waves induced by the positive WSCAs over the western Pacific and the negative WSCAs centered around 140°W south of 5°N, respectively (Figures 2b2–2b5), counteract each other in the western central Pacific, which results in the absence of reflected upwelling Kelvin waves at the western boundary. Meanwhile, the easterly anomalies east of 160°W (Figure 3b) shoal the thermocline and cancel the eastward propagation of the positive ADT-HAs induced by the westerly anomalies in the CP (Hameed et al., 2018; Kug et al., 2009). The above two effects result in the stagnant feature of ADT-HAs during the CP El Niño.

The above analyses suggest that the different impacts of EP and CP El Niño on the NECC are the result of the different oceanic responses excited by the distinct WSCAs patterns associated with the two El Niño types. In Figure 3, we regress the interannual wind stress anomalies and WSCAs onto the EPI and CPI, respectively. The WSCAs are dominated by the meridional gradient of the zonal wind stress (Figures 3c–3f). Figures 3a and 3b also reveal how the main WSCA patterns of the EP and CP El Niño that we used to explain the different impacts on the NECC in Figure 2 are linked to the zonal wind stress anomaly patterns. Figure 3a shows that the EP El Niño is accompanied by large westerly anomalies in the tropical CP, which induce positive values of WSCAs to the south of equator in (Figures 2a2–2a5). The positive WSCAs are primarily responsible to affect the NECC via oceanic wave propagations. As for the CP El Niño (Figure 3b), the surface wind anomalies are dominated by westerly anomalies over the tropical western Pacific and easterly anomalies over the tropical EP. These two anomaly centers are responsible for producing the positive values in the WSCAs over the western Pacific and the negative values over the EP north of the equator (Figures 2b2–2b5).

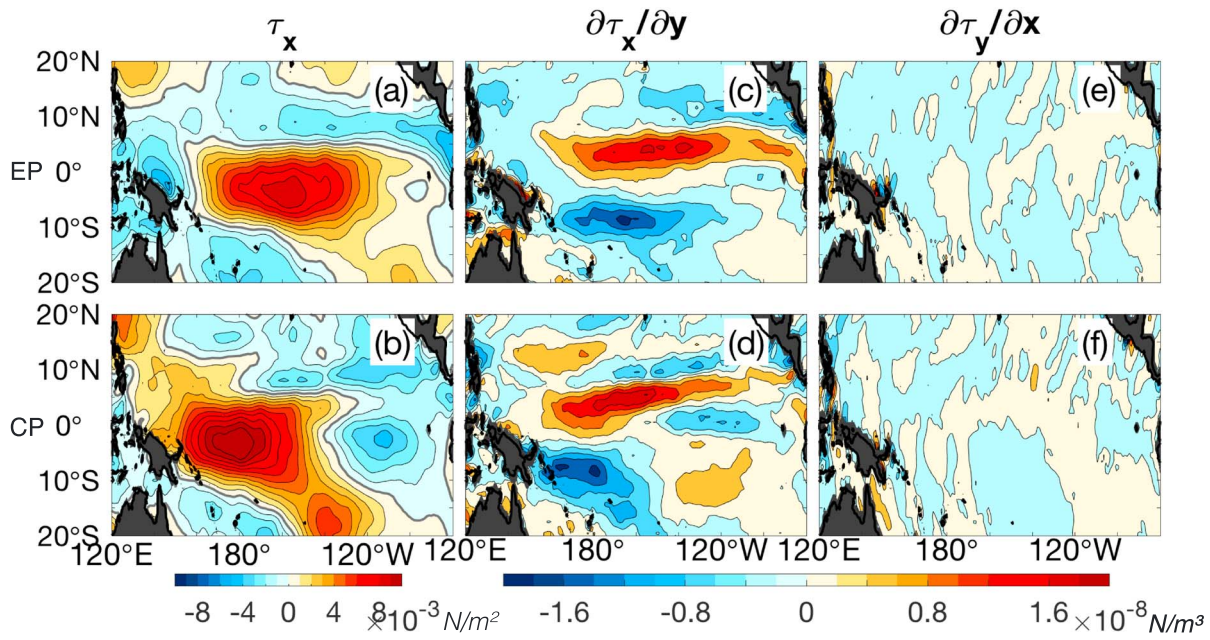

Figure 3. Interannual anomalies in the ERA-Interim zonal wind stress (a and b), meridional gradient of zonal wind stress (c and d), and zonal gradient of meridional wind stress (e and f) regressed onto the EP index (upper panels) and CP index (lower panels). Units and contour intervals are Newton per square meter and 10^{-3} N/m^2 respectively in (a, b) and Newton per cubic meter and 2×10^{-9} N/m^3 respectively in (c–f). CP = central Pacific; EP = eastern Pacific.

To more rigorously examine the oceanic response to the wind forcing, we performed numerical experiments with a 1.5-layer reduced-gravity ocean model (see supporting information Texts S3 and S4 for details) forced by the wind stress anomalies regressed onto the EPI and CPI, respectively. We can see that the model is able to realistically reproduce the observed sea level variations during the period 1993–2016 (Figure S1). The linear correlation between the observed and modeled SLA averaged between 4°N and 6°N is 0.89 (Figure S2), suggesting the reliability of the model in capturing the interannual SLAs in this region. In particular, the model nicely simulates the observed SLAs in the equatorial Pacific during the strongest EP and CP El Niño events: the 1997/1998 EP El Niño and the 2009/2010 CP El Niño (Figure S3). Therefore, we performed twin experiments using the EPI and CPI-regressed wind stress forcing to simulate the 1997/1998 and 2009/2010 El Niño, respectively. Here we call the twin experiments as EP-Wind Stress Anomaly (EP-WSA) and CP-WSA, respectively, which aim to examine how the ocean responds to the wind stress forcing associated with the EP and CP El Niño.

We compare in Figure 4 the modeled and observed evolution of SLAs (color) and velocity (vector) anomalies (UAs) during these two events. The most obvious features are that the observed evolution is captured by the EP-WSA experiment for the 1997/1998 El Niño (cf. Figures 4a–4c/4d–4f) and by the CP-WSA experiment for the 2009/2010 El Niño (cf. Figures 4j–4l/4p–4r). For the 1997/1998 event, the EP-WSA experiment (Figures 4d–4f) reproduces the most observed intensification and southward shift of the NECC (indicated by the eastward current anomalies south of the climatological position of the NECC's axis) in the central eastern Pacific and the accompanying propagation of positive SLAs. The observed negative SLAs and westward UAs in the western Pacific are also simulated. The CP-WSA experiment (Figures 4g–4i) fails to capture these major observed features. It is worth noting that the EP-WSA experiment fails to reproduce the negative SLAs east of Philippine Islands during the event, which suggests that SLA variations in this region are probably determined by local wind forcing that contains variability not fully represented by the ENSO signal (Qiu & Chen, 2010).

For the 2009/2010 El Niño, the CP-WSA experiment (Figures 4p–4r) shows an intensified and southward shifted NECC in the western central Pacific that is close to what was observed (Figures 4j–4l). The observed positive SLAs east of the Philippine Islands near 10°N and the positive values along the equator east of the dateline are also reproduced. In comparison, the EP-WSA experiment (Figures 4m–4o) fails to reproduce the observed changes in the NECC during this event. Although there are some differences between the observations and simulations in both twin experiments for 1997/1998 and 2009/2010 events, the total

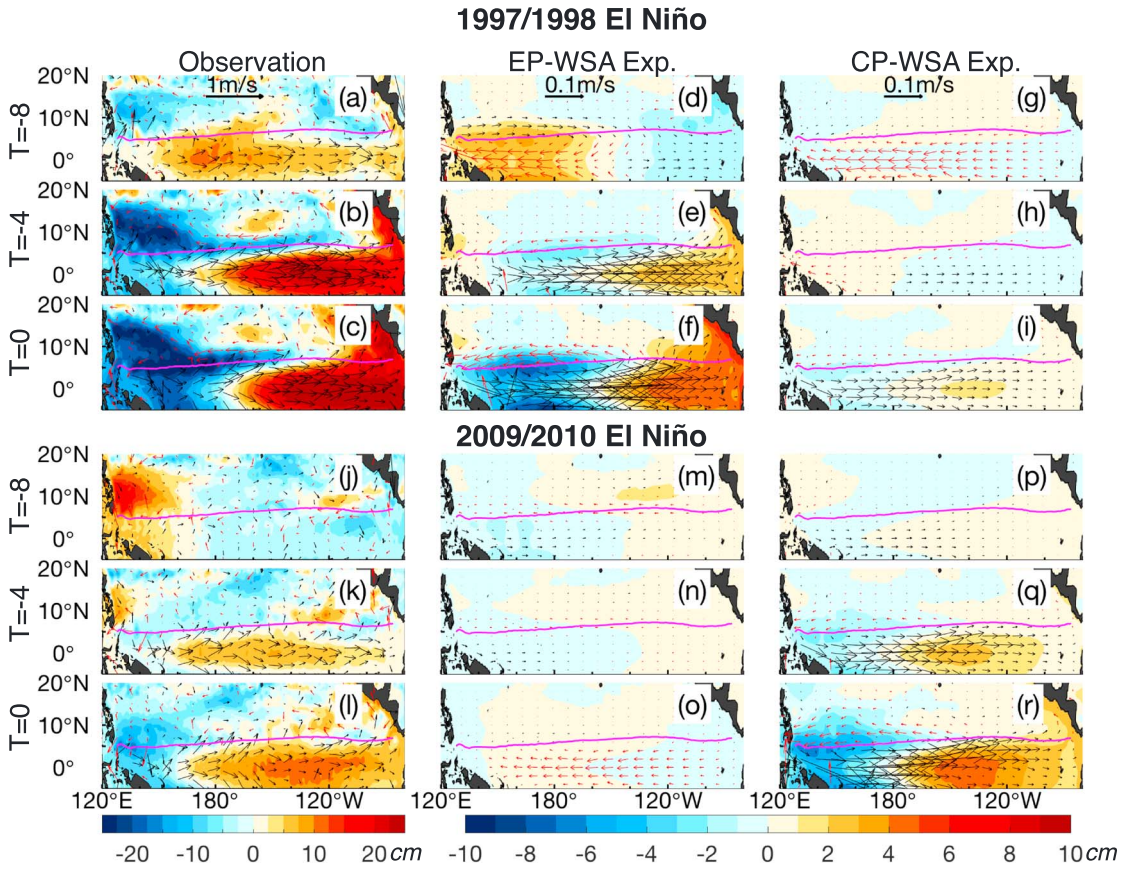

Figure 4. Evolution of the ADT-HAs (color shading; cm) and ADT-UVAs (m/s) during the 1997/1998 (upper panels) and 2009/2010 (lower panels) El Niño events from the observations (a–c and j–l), the EP-WSA experiment (d–f and m–o), and the CP-WSA experiment (g–i and p–r). Magenta lines denote the mean location (Y_{CM}) of the North Equatorial Counter Current calculated from the altimeter observations during the period 1993 to 2016. $T = 0$ denotes the peak month for each El Niño event. CP = central Pacific; EP = eastern Pacific.

wind stress experiments can reproduce quite well the observed features (Figure S3), suggesting the reliability of the model in capturing the interannual signals in this region.

The forced ocean model experiments further confirm that the different wind stress forcing associated with the different central locations of SSTA is the primary reason why the EP and CP types of El Niño produce different impacts on the NECC.

4. Conclusions

Using observational analyses and ocean model experiments, we show that both CP and EP types of El Niño can exert significant but different impacts on the interannual variations of the NECC. This conclusion differs from that of a previous study (HQ12), which suggested that only EP El Niño can significantly impact the NECC. We find this to be due to the fact that HQ12 classified some events that we consider to be of the CP type as EP type events. Impacts on NECC by CP El Niño were included as part of the EP El Niño impact in their study. To make sure that our results are not dependent on the type classification in the composite analyses, we also performed correlation analyses and numerical experiments to further confirm our findings.

We find that the two types of El Niño produce comparable but different spatial structures in the anomalies of the surface wind stress forcing giving rise to distinct impacts on the NECC. The wind forcing during the EP El Niño induces an area of positive SLAs south of the climatological position of the NECC in the EP, which displaces the NECC southward and intensifies it in the central eastern Pacific. In contrast, the wind stress forcing during the CP El Niño induces a region of negative SLAs north of the NECC in the western Pacific and a region

of positive SLAs south of the NECC in the CP. This SLA pattern causes the NECC to shift southward and intensify in the western central Pacific. Ekman pumping, oceanic Kelvin and Rossby wave propagation, and geostrophic balance are involved in the dynamical mechanism that links the El Niño wind stress forcing to the NECC fluctuations.

This study suggests that ENSO diversity is important in the studies of NECC variability and that the El Niño type needs to be considered in studies of the relationships between El Niño and the NECC or the oceanic responses to El Niño.

Acknowledgments
We thank two anonymous reviewers for their valuable comments. We acknowledge the Copernicus Marine and Environment Monitoring Service and the European Centre for Medium-Range Weather Forecasts for sharing the data. The work is supported by the grants NSFC (41876009), QNLM (2016ASKJ12), and NSFC (41421005, 41720104008, and 41376032).

References

Ashok, K., Behera, S. K., Rao, S. A., Weng, H., & Yamagata, T. (2007). El Niño Modoki and its possible teleconnection. *Journal of Geophysical Research*, *112*, C11007. https://doi.org/10.1029/2006JC003798

Balmaseda, M. A., Mogensen, K., & Weaver, A. T. (2013). Evaluation of the ECMWF ocean reanalysis system ORAS4. *Quarterly Journal of the Royal Meteorological Society*, *139*(674), 1132–1161. https://doi.org/10.1002/qj.2063

Berrisford, P., Dee, D., Poli, P., Brugge, P., Fielding, K., Fuentes, M., et al. (2011). The ERA-Interim archive version 2.0. ERA Report Series 1, ECMWF, Shinfield Park. Reading, UK, 13177

Delcroix, T., Eldin, G., Radenac, M. H., Toole, J., & Firing, E. (1992). Variation of the western equatorial Pacific Ocean, 1986–1988. *Journal of Geophysical Research*, *97*(C4), 5423–5445. https://doi.org/10.1029/92JC00127

Donguy, J. R., & Meyers, G. (1996). Mean annual variation of transport of major currents in the tropical Pacific Ocean. *Deep Sea Research Part I: Oceanographic Research Papers*, *43*(7), 1105–1122. https://doi.org/10.1016/0967-0637(96)00047-7

Gouriou, Y., & Toole, J. (1993). Mean circulation of the upper layers of the western equatorial Pacific Ocean. *Journal of Geophysical Research*, *98*(C12), 22,495–22,520. https://doi.org/10.1029/93JC02513

Hameed, S. N., Jin, D., & Thilakan, V. (2018). A model for super El Niños. *Nature Communications*, *9*(1), 2528. https://doi.org/10.1038/s41467-018-04803-7

Hsin, Y. C., & Qiu, B. (2012). The impact of eastern-Pacific versus central-Pacific El Niños on the North Equatorial Countercurrent in the Pacific Ocean. *Journal of Geophysical Research*, *117*, C11017. https://doi.org/10.1029/2012JC008362

Johnson, G. C., Sloyan, B. M., Kessler, W. S., & McTaggart, K. E. (2002). Direct measurements of upper ocean currents and water properties across the tropical Pacific during the 1990s. *Progress in Oceanography*, *52*(1), 31–61. https://doi.org/10.1016/S0079-6611(02)00021-6

Kao, H. Y., & Yu, J. Y. (2009). Contrasting eastern-Pacific and central-Pacific types of ENSO. *Journal of Climate*, *22*(3), 615–632. https://doi.org/10.1175/2008JCLI2309.1

Kessler, W. S., & Taft, B. A. (1987). Dynamic heights and zonal geostrophic transports in the central tropical Pacific during 1979–84. *Journal of Physical Oceanography*, *17*(1), 97–122. https://doi.org/10.1175/1520-0485(1987)017<0097:DHAZGT>2.0.CO;2

Kug, J. S., Jin, F. F., & An, S. I. (2009). Two types of El Niño events: Cold tongue El Niño and warm pool El Niño. *Journal of Climate*, *22*(6), 1499–1515. https://doi.org/10.1175/2008JCLI2624.1

Larkin, N. K., & Harrison, D. E. (2005). On the definition of El Niño and associated seasonal average US weather anomalies. *Geophysical Research Letters*, *32*, L13705. https://doi.org/10.1029/2005GL022738

Livezey, R. E., & Chen, W. Y. (1983). Statistical field significance and its determination by Monte Carlo techniques. *Monthly Weather Review*, *111*(1), 46–59. https://doi.org/10.1175/1520-0493(1983)111<0046:SFSAID>2.0.CO;2

Masunaga, H., & L'Ecuyer, T. S. (2011). Equatorial asymmetry of the East Pacific ITCZ: Observational constraints on the underlying processes. *Journal of Climate*, *24*(6), 1784–1800. https://doi.org/10.1175/2010JCLI3854.1

Meyers, G., & Donguy, J. R. (1984). The North Equatorial Countercurrent and heat storage in the western Pacific Ocean during 1982–83. *Nature*, *312*(5991), 258. https://doi.org/10.1038/312258a0–260.

Mogensen, K., Alonso Balmaseda, M., & Weaver, A. (2012). The NEMOVAR ocean data assimilation system as implemented in the ECMWF ocean analysis for system 4. *ECMWF Technical Memorandum*, *66*, 59.

Philander, S. G. H., Hurlin, W. J., & Seigel, A. D. (1987). Simulation of the seasonal cycle of the tropical Pacific Ocean. *Journal of Physical Oceanography*, *17*(11), 1986–2002. https://doi.org/10.1175/1520-0485(1987)017<1986:SOTSCO>2.0.CO;2

Qiu, B., & Chen, S. (2010). Interannual variability of the North Pacific Subtropical Countercurrent and its associated mesoscale eddy field. *Journal of Physical Oceanography*, *40*(1), 213–225. https://doi.org/10.1175/2009JPO4285.1

Qiu, B., & Joyce, T. M. (1992). Interannual variability in the mid-and low-latitude western North Pacific. *Journal of Physical Oceanography*, *22*(9), 1062–1079. https://doi.org/10.1175/1520-0485(1992)022<1062:IVITMA>2.0.CO;2

Ren, H. L., & Jin, F. F. (2011). Niño indices for two types of ENSO. *Geophysical Research Letters*, *38*, L04704. https://doi.org/10.1029/2010GL046031

Reverdin, G., Frankignoul, C., Kestenare, E., & McPhaden, M. J. (1994). Seasonal variability in the surface currents of the equatorial Pacific. *Journal of Geophysical Research*, *99*(C10), 20,323–20,344. https://doi.org/10.1029/94JC01477

Richards, K. J., Xie, S. P., & Miyama, T. (2009). Vertical mixing in the ocean and its impact on the coupled ocean–atmosphere system in the eastern tropical Pacific. *Journal of Climate*, *22*(13), 3703–3719. https://doi.org/10.1175/2009JCLI2702.1

Shi, N., Wei, F. Y., Feng, G. L., & Sheng, T. L. (1997). Monte Carlo test used in correlation and composite analysis of meteorological fields. *Journal of Nanjing Institute of Meteorology*, *20*(3), 355–359. https://doi.org/10.13878/j.cnki.dqkxxb.1997.03.011

Wyrtki, K. (1979). The response of sea surface topography to the 1976 El Niño. *Journal of Physical Oceanography*, *9*(6), 1223–1231. https://doi.org/10.1175/1520-0485(1979)009<1223:TROSST>2.0.CO;2

Wyrtki, K., & Kendall, R. (1967). Transports of the Pacific equatorial countercurrent. *Journal of Geophysical Research*, *72*(8), 2073–2076. https://doi.org/10.1029/JZ072i008p02073

Yu, J. Y., & Kao, H. Y. (2007). Decadal changes of ENSO persistence barrier in SST and ocean heat content indices: 1958–2001. *Journal of Geophysical Research*, *112*, D13106. https://doi.org/10.1029/2006JD007654

Yu, J. Y., & Kim, S. T. (2010). Three evolution patterns of central-Pacific El Niño. *Geophysical Research Letters*, *37*, L08706. https://doi.org/10.1029/2010GL042810

Yu, Z., McCreary, J. P. Jr., Kessler, W. S., & Kelly, K. A. (2000). Influence of equatorial dynamics on the Pacific North Equatorial Countercurrent. *Journal of Physical Oceanography*, *30*(12), 3179–3190. https://doi.org/10.1175/1520-0485(2000)030<3179:IOEDOT>2.0.CO;2

Zhao, J., Li, Y., & Wang, F. (2013). Dynamical responses of the West Pacific North Equatorial Countercurrent (NECC) system to El Niño events. *Journal of Geophysical Research: Oceans*, *118*, 2828–2844. https://doi.org/10.1002/jgrc.20196